Nanotechnology in Biomaterials

JOURNAL OF
biomaterials
applications

Journal of Biomaterials Applications
2016, Vol. 31(3) 366–378

DOI: 10.1177/0885328216646910
jba.sagepub.com
SAGE

Potent antimicrobial and antibiofilm activities of bacteriogenically synthesized gold–silver nanoparticles against pathogenic bacteria and their physiochemical characterizations

Mohankandhasamy Ramasamy, Jin-Hyung Lee and Jintae Lee

Abstract

The objective of this study was to develop a bimetallic nanoparticle with enhanced antibacterial activity that would improve the therapeutic efficacy against bacterial biofilms. Bimetallic gold–silver nanoparticles were bacteriogenically synthesized using γ-proteobacterium, *Shewanella oneidensis* MR-1. The antibacterial activities of gold–silver nanoparticles were assessed on the planktonic and biofilm phases of individual and mixed multi-cultures of pathogenic Gram negative (*Escherichia coli* and *Pseudomonas aeruginosa*) and Gram positive bacteria (*Enterococcus faecalis* and *Staphylococcus aureus*), respectively. The minimum inhibitory concentration of gold–silver nanoparticles was 30–50 μM than that of other nanoparticles ($>$100 μM) for the tested bacteria. Interestingly, gold–silver nanoparticles were more effective in inhibiting bacterial biofilm formation at 10 μM concentration. Both scanning and transmission electron microscopy results further accounted the impact of gold–silver nanoparticles on biocompatibility and bactericidal effect that the small size and bio-organic materials covering on gold–silver nanoparticles improves the internalization and thus caused bacterial inactivation. Thus, bacteriogenically synthesized gold–silver nanoparticles appear to be a promising nanoantibiotic for overcoming the bacterial resistance in the established bacterial biofilms.

Keywords

Biological synthesis, *Shewanella oneidensis*, bimetallic nanoparticles, antibacterial, antibiofilm, electron microscope, Au–Ag NPs

Introduction

Antibacterial agents either inhibit bacterial growth or kill bacteria, ideally without harming surrounding tissues or the environment. Most antibacterial agents are either natural products, chemically modified natural compounds or synthetics. Long-term use of these agents caused the worldwide emergence of inherent antibiotic resistance in pathogens, which possessed a serious life-threatening issue.[1] In addition, the formation of biofilms produced by sessile microbial communities is responsible for a multitude of chronic diseases associated with biomedical devices.[2,3] Biofilms represent an impermeable shield and are more tolerant of chemicals, detergents, disinfectants, and traditional antibiotic therapies and cause multidrug resistance (MDR).[4,5] Due to the fact that bacteria have developed MDR, bacteria residing within the protected biofilm structures have emerged as a potential cause for lethal infections and increases morbidity, which are the greatest health challenges worldwide. Clearly, developing antimicrobial agents that either kill the bacteria or prevent and disrupt the pathogenic biofilm are a pressing emergence to alleviate healthcare-related infections. Hence, we have prompted the development of alternative nanotechnological approach to control or treat bacterial infections.

School of Chemical Engineering, Yeungnam University, Gyeongsan, Republic of Korea

Corresponding author:
Jintae Lee, School of Chemical Engineering, Yeungnam University, Gyeongsan 38541, Republic of Korea.
Email: jtlee@ynu.ac.kr

Recently, nanotechnology-based antimicrobial agents have contributed to efforts to combat microbial infections. In biomedical research, metallic and metal oxide nanoparticles (NPs) are being extensively investigated due to their ability to use different mechanisms to kill pathogenic bacteria.[6–8] Silver-containing systems, including silver nanoparticles (Ag NPs), are currently viewed as promising disinfectants for a wide range of microorganisms and have been utilized in many consumer products.[9–11] In particular, the development of multi-metallic composite materials in combination with biocompatible nanomaterials that act as antibacterial reservoirs offers a means of improving antibacterial efficacy.[12] Bimetallic nanoparticle technology has attention because of complex electron-associated interaction mechanisms between electron rich (metallic) elements. Bimetallic/bimetal oxide NPs, such as, Au–Pd, ZnO-MgO, Fe-Pt, Au–Ag, and Au–Pt NPs, have potential applications in catalysis, sensors, imaging, drug delivery, and optoelectronics,[13–16] and of these, Au–Ag bimetallic NPs might have interesting bactericidal properties because the Ag could be leached into the immediate environment. Banerjee et al.[17] tested the antibacterial efficacy of chemically synthesized bimetallic Au–Ag core-shell NPs, but the biofabrication of Au–Ag NPs and their antibacterial applications remained unexplored.

Various techniques have been used to prepare bimetallic Au–Ag NPs, such as, chemical reduction, radiation-induced synthesis, electrochemical synthesis, sonochemical synthesis, and green synthesis,[18–24] and recently, biological routes to the biosynthesis of nanomaterials based on the reduction of metal ions into stable NPs, including bimetallic NPs, have been devised.[25–30] However, the biological syntheses of bimetallic nanostructures containing Au and Ag based on the co-precipitation of the two metals from solution by bacteria have not been previously described. Microorganisms have been known as important nanofactories which hold immense potential as eco-friendly and economic tool, avoiding toxic chemicals and require less energy to produce biocompatible NPs in short time than physiochemical methods. In the past years, bacteria have been utilized for the extra- and intracellular synthesis of NPs. An array of bacteria-mediated protocols for NP synthesis has been reported using bacteria biomass, supernatant of the media, and derived components. In particular, extracellular synthesis has received much focus because it eliminates the cumbersome processing steps of NP purification involved in other methods. Moreover, metal-resistant proteins, peptides, genes, enzymes, and organic materials have significant involvement as inherent bioreductant to transform inorganic metal ions into metal NPs by biochemical processes. Furthermore, these factors help in providing natural capping, thereby preventing them from aggregation and helping the NPs to remain stable for a long time with improved stability. These abilities of microorganisms to interact, extract, accumulate, or precipitate the metallic ions have been capitalized in a number of commercial biotechnology applications such as biomineralization, bioremediation, biosorption, and bioleaching. Importantly, the lack of knowledge in the exact mechanism involved in NP synthesis, yield of NPs corresponding to metal salts, polydispersity, and biocompatibility are the major limitations of the bacteriogenic synthesis method which needs considerable investigation to produce NPs with higher efficacy.[31,32]

The aim of this study was to synthesize bimetallic NPs using viable *S. oneidensis* MR-1 and to analyze their antibacterial capability against pathogenic bacteria. After bacterial reduction, the nanostructures obtained were studied optically, morphologically, and structurally using UV-Visible spectroscopy (UV-Vis), particle size and zeta potential analysis using dynamic light scattering measurements (DLS), X-ray diffraction (XRD), X-ray photoelectron spectroscopy (XPS) and high-resolution transmission electron microscopy (HRTEM) embedded with EDX. The severity of the antibacterial effects of Au–Ag NPs on bacteria was visualized by field emission scanning electron microscopy (FESEM) and transmission electron microscopy (TEM).

Materials and methods

Bacterial strains and growth conditions

The bacterial strains used were *S. oneidensis* MR-1, *E. coli* O157:H7 [ATCC43895, EDL933], *E. faecalis*, *P. aeruginosa* PAO1, and *S. aureus* (ATCC 6538). Bacterial cells were initially streaked from –80°C glycerol stock on Luria–Bertani agar (LBA) plates at 37°C. After overnight growth, a single colony was inoculated in 25 ml of fresh LB broth in a 250 ml Erlenmeyer flask and incubated on a rotary shaker (at 250 r/min) for 24 h at 30°C. For phenotypic assays, overnight cultures (stationary phase cells) were re-inoculated into LB broth at an initial turbidity of 0.05 and an optical density of 600 nm (OD_{600}). All chemicals and reagents used in this study were purchased from Sigma-Aldrich (St. Louis) and used as received.

Biofabrication of Au–Ag NPs

Overnight grown *S. oneidensis* MR-1 was collected by centrifugation ($1087 \times g$, 25°C, 20 min), washed three times with sterile deionized water, and re-suspended in a 250 ml bottle containing sodium lactate. $HAuCl_4 \cdot 4H_2O$ and $AgNO_3$ (1 ml; both as 10^{-3} M solutions) were then simultaneously added and incubated in the

dark with shaking (at 250 r/min) at 37°C. NPs formation was monitored visually by color change from colorless to brownish-violet, and by UV-Vis absorption spectroscopy. The reaction suspension was then autoclaved for 15 min at 121°C, centrifuged at 1932 × *g* for 10 min, and finally filtered through a sterile 0.45 μM syringe filter. As-formed Au–Ag NPs were collected by centrifugation at 48,298 × *g* for 30 min. After washing twice with distilled water, the Au–Ag alloy nanoparticles were used for further studies.

Preparation of NPs using S. oneidensis MR-1 biofilm (bio-NPs)

An electrochemically active biofilm (EAB) of *S. oneidensis* MR-1 was formed on carbon paper in mineral salt medium containing sodium acetate as substrate.[33] Initially, under anaerobic conditions, 10 ml of grown bacteria was added, and the medium was replaced with fresh medium twice per week. The biofilm produced was separated and hung in mineral salt medium containing $HAuCl_4 \cdot 4H_2O$ and $AgNO_3$ (1 ml; both as 10^{-3} M solutions) with magnetic stirring at 30°C in the dark.

Synthesis of Au NPs

Au NPs were synthesized as previously described method with minor modifications.[34] Briefly, 1.25 ml of 10^{-3} M $HAuCl_4 \cdot 4H_2O$ was mixed into 50 ml of boiling water, 1.7 ml of 10^{-3} M trisodium citrate trihydrate solution was then added with stirring, and the mixture was refluxed for 30 min until the color changed to a permanent pinkish-purple, indicating Au NP formation. It was then cooled and filtered using a 0.22 μm syringe filter and stored at 4°C for further use.

Characterizations

Absorbance spectra of NPs were obtained using an UV-Visible spectrophotometer (UV-1800, Shimadzu, Japan). A NanoZS dynamic light-scattering particle size analyzer (Malvern Instruments, Malvern, UK) was used to determine average particle size (nm), polydispersity index (PDI), zeta potential (mV), and NP stability. NP morphology was determined by HRTEM (Tecnai G2 F20, FEI, USA) at an accelerating voltage of 200 kV, and quantitative elemental analysis was performed by energy dispersive X-ray spectrometry (EDS) embedded in the HRTEM. From TEM images, the particle size distributions of Au–Ag NPs were calculated by averaging 200 particles using IMAGE J software (developed by National Institutes of Health, Bethesda, MD, USA). Thin film XRD patterns were recorded on a diffractometer (PANalytical, X'Pert-PRO MPD) and compared with those of standard compounds in the JCPDS data file. X-ray photoelectron spectra (XPS) were collected using ESCALAB 250 XPS System (Thermo Fisher Scientific UK).

Antimicrobial assays

Determination of minimum inhibitory concentration

The effects of Au–Ag NPs, Au NPs, and bio-NPs on bacteria were assessed by minimum inhibitory concentration (MIC) determination using the standard broth microdilution method. As-synthesized NPs were tested in microbial cultures of (*E. coli*, *E. faecalis*, *P. aeruginosa*, *and S. aureus*) and of the multi-culture strain (i.e. mixture of all above mentioned bacteria). In brief, sterile LB media containing different concentrations of NPs (10–50 μM) were sonicated for 10 min to prevent aggregation and ensure complete NP dispersion. Subsequently, they were inoculated with a freshly prepared, overnight grown bacterial suspension at 10^4–10^5 colony-forming units per ml (CFU/ml), and incubated at 37°C in a shaking incubator at 250 r/min for 24 h. Turbidity values were then measured at OD_{600} using an Optizen (2120UV) UV/Vis spectrophotometer. NPs in medium without bacteria were used as positive controls, and bacteria inoculum in medium without Au–Ag NPs were used as negative controls. The absorbance values of positive controls were subtracted from the sample values.

Disk diffusion test

Bacterial sensitivity to antibacterial agents is commonly assessed using a disk diffusion test and standard antibiotic impregnated disks. A similar approach was adopted to examine the bactericidal activities of Au–Ag NPs, Au NPs, bio-NPs, and streptomycin against the four individual and multi-culture test strains on LBA plates by measuring zones of inhibition (ZIs). Initially, different NPs and antibiotic laden filter paper disks (5 mm) were prepared by drying in an oven for 1 h. Bacterial suspensions (100 μl; 10^4–10^5 CFU/ml) were evenly spread on the surfaces of LBA plates to obtain uniform bacterial distributions, and then NPs and antibiotic-loaded filter paper disks (5 per plate) were placed on the plates. Finally, the culture plates were incubated at 37°C for 24 h, and average diameters of ZIs were measured using a ruler.

Biofilm assay

A static biofilm assay for Au–Ag NPs, Au NPs, and bio-NPs was performed on 96-well polystyrene plates (SPL Life Sciences, Korea) for individual and mixed multi-culture strains of *E. coli*, *E. faecalis*, *P. aeruginosa*,

and *S. aureus*. In brief, overnight grown cultures were adjusted to an OD_{600} of 0.05 in LB medium containing NPs at concentrations of 0–250 µM and incubated for 24 h without shaking at 37°C. Plates were then washed with water to remove any planktonic cells. Excess water was removed, and then each well was filled with 300 µl of crystal violet (0.1% v/v). After incubation for 30 min at room temperature, the plates were emptied, washed three times with water, blotted onto a tissue paper towels to remove excess dye and dried. Ethanol was then added to each well to solubilize the crystal violet. Finally, total biofilm formation was assessed by measuring absorbance at 570 nm (OD_{570}) using a Thermo Scientific Multiskan EX (Thermo Fisher Scientific, Vantaa, Finland). The results are the means and standard deviations (SD) of three replicate tests.

Electron microscopic analysis of the effect of NPs on cellular morphology

Preparation of cells of FESEM

E. coli, *E. faecalis*, or *P. aeruginosa* in the mid-exponential phase were suspended in LB medium containing Au–Ag NPs or Au NPs in the sterile Erlenmeyer flasks. Untreated control bacteria were prepared in separate LB medium. Cultures were incubated at 37°C with shaking at 250 r/min for 12 h, and cells were then pre-fixed using a glutaraldehyde (2.5%) and formaldehyde (2%) mixture. They were then filtered through 0.45 µm nylon filter and washed with 0.2 M phosphate buffer. Filter papers containing cells were kept overnight at 4°C in phosphate buffer and then post-fixated with 2% osmium tetroxide and dehydrated using an ethanol series (50 to 99.9% v/v). Cells were then placed in isoamyl acetate, dried using a critical point dryer (HCP-2, Hitachi, Japan), sputter coated using a gold ion-sputter (E-1030, Hitachi, Japan), and imaged under a FESEM (S-4200, Hitachi, Japan) at 5 kV.

Preparation of cells for TEM

Morphological changes of *E. coli* at predetermined time intervals (0.5–2 h) after NPs treatment were examined as previously described with modifications.[35] Initially, *E. coli* was grown and incubated with a lethal dose of Au–Ag NPs for 2 h. Then in the pre-fixation process, cells were treated by adding an aldehyde mixture to sample media and kept overnight at 4°C. Cells were then collected by centrifugation and post-fixed with 2% osmium tetroxide overnight at 4°C, and washed three times by centrifugation using 0.2 M phosphate buffer. Cell pellets were mixed with 2% agarose in sterile tube to form a cell block, which was sliced to the desired size. Slices were dehydrated with graded ethanol (50 to 99.9% v/v) for 20 min. Slices were then embedded in an Epon resin mixture (Hatfield, USA), which was polymerized at different temperatures to ensure complete polymerization. Embedded cell containing slices were then sectioned using a MT-X ultramicrotome (Tucson, USA), then loaded onto TEM copper grids. It was stained with uranyl acetate and treated with lead citrate to remove any traces of moisture. Microscopy was performed with H-7600 electron microscope (Tokyo, Japan) at 120 keV.

Results and discussion

Synthesis and characterization of Au–Ag NPs

The primary focus of this present work was to synthesis bimetallic Au–Ag NPs by metal-reducing bacteria with better antibacterial/antibiofilm activities against pathogens, as an alternative to conventional antibiotics (as sketched in Figure 1). Uni- and multi-cellular microorganisms sequester metals intracellularly or secrete them into the external environment, and thus, we used this essentially defensive mechanism to fabricate nanomaterials under ambient conditions.[27] Although reports have been published on the synthesis and applications of bacteriogenic monometallic NPs, no report has been issued on the synthesis of bimetallic NPs or on their antibiofilm properties.

In this study, while experimenting different ratios (1:1, 2:1 and 3:1) of Au to Ag precursors, the SPR and size of the Au NPs were unchanged (data not shown), equimolar concentrations of Au or Ag formed considerable amount of Ag deposition on the Au to form stable bimetallic sols. In contrast, increasing the concentration of Ag never formed stable bimetallic sols, and hence a distinct antibacterial property could not be achieved. These observations were in corroboration with the reports. Hence, metal precursors of Au and Ag at a molar ratio of 1:1 were chosen as a suitable concentration. Then it was added to *S. oneidensis* MR-1 culture, the reaction mixture changed from pale yellow to brownish violet and the corresponding UV-Vis spectra exhibited (Figure 2) an SPR band at 510 nm, that is, between the standard absorption maxima (λ_{max}) of nanogold (540 nm) and nanosilver (410 nm), respectively, indicating the alloy formation.[36,37] The complete disappearance of the SPR band of nanosilver indicated that the formed bimetallic nanostructure had a uniform distributions of Au and Ag. Further, as shown in Figure 2 (inset), the color of NP dispersions and the single SPR peaks at 540 and 590 nm indicated the formation of Au NPs and monometallic bio-NPs. Since bio-NPs produced a different color, a broader λ_{max} at ~620 nm, and had no

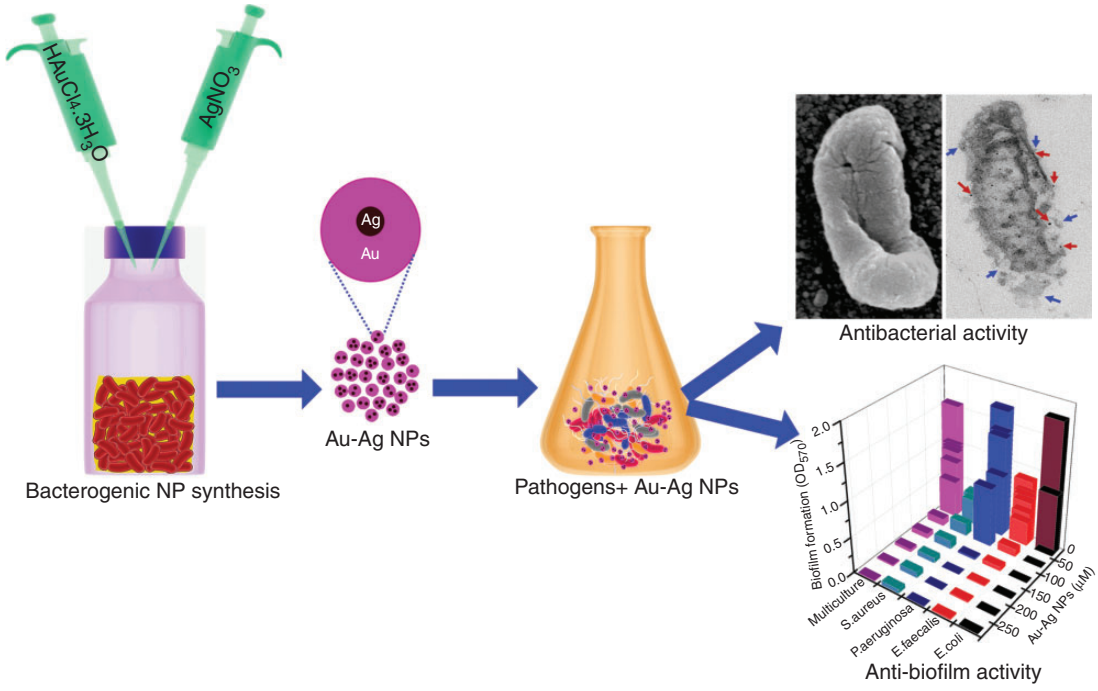

Figure 1. Au–Ag NP synthesis through the simultaneous reduction of Au and Ag precursors using *S. oneidensis MR-1*. Antimicrobial applications like, bactericidal effect and biofilm inhibitions of Au–Ag NPs have illustrated schematically.

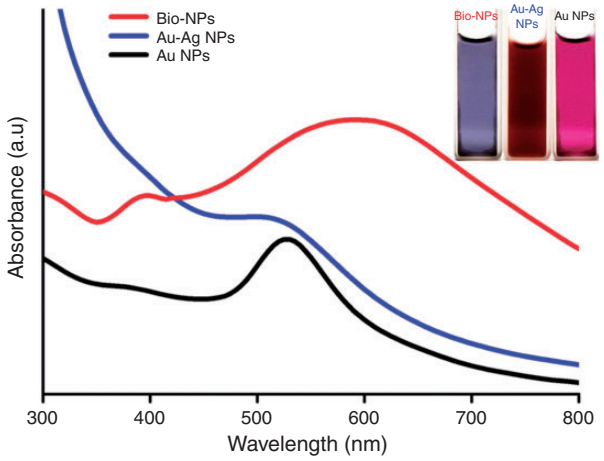

Figure 2. Physicochemical characteristics of NPs. UV-Visible absorbance spectra of dispersions containing Au NP (black) synthesized by chemical reduction method, spherical Au–Ag NP (blue) produced by biological reduction using *S. oneidensis* and Bio-NPs (red) of large aspect ratio synthesized using active biofilm method. Insets show the colors of each NP dispersions.

antibacterial effect this confirmed the formation of monometallic nanostructures. From the micrometer-sized bio-NPs, it was concluded that the single strain EAB biofilm of *S. oneidensis* MR-1 was incapable of reducing metal precursors to form bimetallic NPs.

DLS analysis of NPs and their stabilities

The average hydrodynamic diameters of as-synthesized Au–Ag NPs, Au NPs, and bio-NPs in water were 209 ± 0.7, 57 ± 3, and 2884 ± 823 nm, with PDIs of 0.157, 0.36, and 0.173, respectively. DLS showed the zeta potential values of Au–Ag NPs, Au NPs, and bio-NPs were -16 ± 0.3, -22 ± 0.4, and -21 ± 0.2 mV, respectively. These negative surface charges indicate that the colloidal NPs are moderately stable.

Au–Ag NP stabilities were assessed in different media for 0- or 6-month period of time by DLS (Figure 3). The size of Au–Ag NPs in water was increased with time from 209 ± 0.7 to 263 ± 2 nm, but the PDI was maintained at same 0.15. On the other hand, the size 175 ± 4 nm in LB medium did not cause any change over six months of incubation that maintained the size of 177 ± 2 nm and a PDI of 0.17. It was observed that Au–Ag NPs in water make aggregation than LB medium. Since Au–Ag NPs were formed using bacteria, the biomass surrounded by NPs could have been interacted with LB medium and improved dispersability and stability, and thus, maintained a particle size smaller. This phenomenon is referred to as the protein corona effect.[38] In contrast, Au–Ag NPs dispersed in ethanol showed a significant particle size change, although the particle size did not exceed 265 ± 3 nm. In this case, the particle size was

considerably lower at 224 ± 2 nm (PDI 0.01) after six months of incubation. This could have been due to an interaction between biomolecules and ethanol or to dissolution. Hence, the biofabricated Au–Ag NPs showed satisfactory colloidal stability in different solvents over prolonged storage.

TEM, HRTEM, and EDS analyses

The TEM and HRTEM images (Figure 4) revealed the sizes and shapes of Au–Ag NPs. As shown in Figure 4(a) and (b), it was indicated that Au–Ag NPs were spherical and had an average particle size distribution of 20 ± 3 nm. TEM measurements showed that NPs were surrounded by an organic biomass, which could explain why DLS determined particle sizes were larger. It has been previously suggested that metal biotransformation involves complex formation with capping proteins, peptides, enzymes, quinones, and electron shuttles which reduces metal ions to the metallic state and subsequently stabilize NPs by coating them with organic materials.[39–41] Further, HRTEM (Figure 4(c)) exhibited the formation of, difference in contrast signals, clear lattice fringes that revealed the presence of highly crystalline Au and Ag on each NPs volume indicating the alloy formation, which concurs with previous reports.[42,43] From the TEM and HRTEM images of bimetallic Au–Ag NPs synthesized by our method, it was clearly noticed that there was a uniform contrast signals for each particle, which confirms the alloy formation with a homogenous electron density thorough out the volume of each particle. The point and ID scan tool of EDS was used to analyze the composition of NPs by individual and collective parts of the NPs. Hence, from the scanning results of different zones in a single NP, we could confirm that the NP uniformly comprised Au and Ag which suggests that they are in alloy form. Furthermore, collective scan result of elemental analysis (Figure 4(d)) indicated the presence of elemental Au (2.2 keV) and Ag (3 keV) in bimetallic Au–Ag NPs and confirmed that the alloy NPs were composed of Au and Ag which was in corroboration with TEM and HRTEM results.

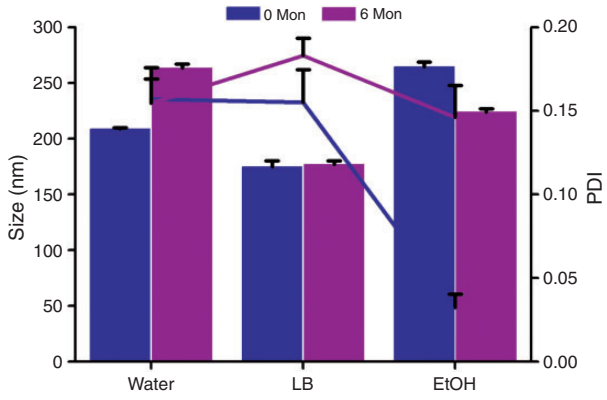

Figure 3. Stability analysis of Au–Ag NPs using dynamic light scattering measurements. Particle size distributions for Au–Ag NPs incubated in water, LB medium, or ethanol for 0 (blue bar) or 6 months (violet bar) with corresponding poly-dispersity indices (blue and violet lines, respectively).

XRD and XPS analysis

The crystalline nature of Au–Ag NPs, Au NPs and bio-NPs was investigated by XRD analysis (Figure 5(a)). For Au–Ag NPs, 2θ peaks at 38.2°, 44.5°, 64.5°, and 78.5° corresponded to the (111), (200), (220), and (311) planes of the face-centered cubic structures.

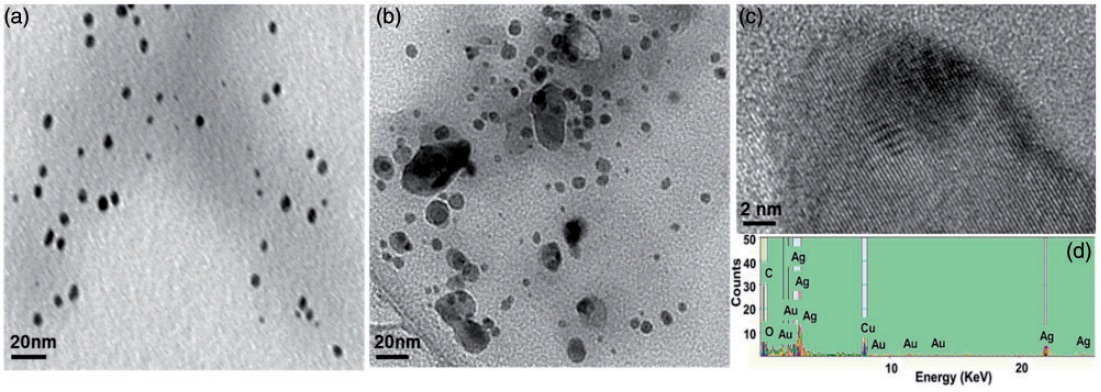

Figure 4. Electron microscopy analysis of Au–Ag NP formation. Transmission electron micrograph of Au–Ag NPs showing bacterial biomass haloes (a), High resolution transmission electron microscopic image of Au–Ag NPs (b), Highly magnified view of Au–Ag NPs showing mixed lattice fringes of Au and Ag (c). Energy dispersive X-ray spectrograph of Au–Ag NPs showing the presence of Au and Ag (d).

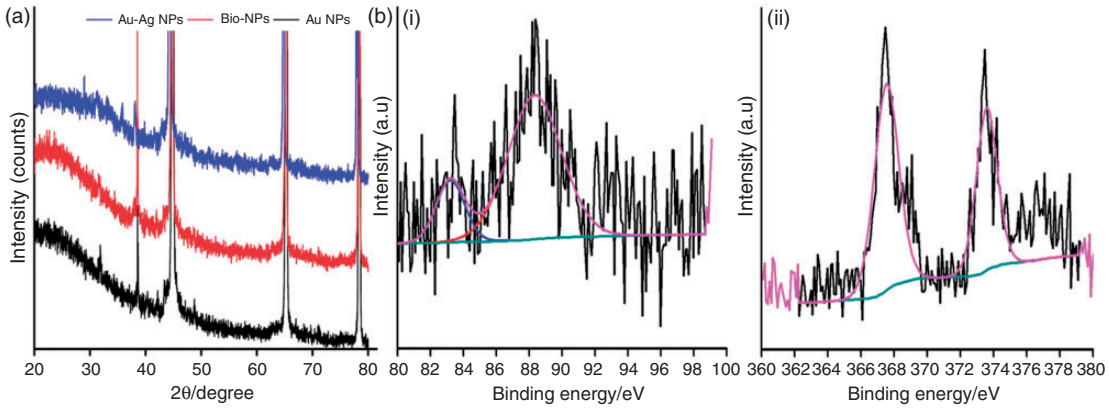

Figure 5. X-ray diffraction patterns of NPs. Thin film X-ray diffractograms of Au–Ag NPs (blue), Au NP (black), and Bio-NPs (red) dispersions in water (a). X-ray photoelectron spectra of Au–Ag NPs (b). Deconvoluted core-level spectra recorded from drop cast Au–Ag NPs B (i and ii). The two spin-orbit components of Au 4f (i) and Ag 3d (ii) are shown for each element.

From XRD measurements, the 2θ values and lattice constants of Au–Ag NPs were found similar to those of Au and Ag because of their similar lattice constants (JCPDS 4-0784 and 4-0783).[44] Importantly, bio-NPs produced XRD patterns similar to Au NPs. In fact, no Ag was observed in bio-NPs, indicating no Au–Ag NPs were formed by EAB. These XRD results confirmed the crystallinity of Au–Ag NPs with a bimetallic structure. The unassigned peaks were tentatively attributed to the crystalline structures of the coating bio-organic phase.[45]

Further, chemical analysis results indicating the alloy formation were supported by XPS analysis. Figure 5(b-i) shows the Au 4f spectrum resolved into two spin-orbit couplings of Au $4f_{7/2}$ and Au $4f_{5/2}$ peaks at binding energy of 84.1 and 87.7 eV, respectively, assigned to Au. Figure 5(b-ii) shows the resolved two spin-orbit couplings of the Ag 3d spectrum of $Ag3d_{5/2}$ and Ag $3d_{3/2}$ peaks at 367.4 and 373.4 eV, respectively, assigned to Ag. Both, Au and Ag spectra, revealed the existence of strong bond between the two metals in the zero valent states (Au^0 and Ag^0), confirming the formation of bimetallic Au–Ag NPs.[29]

Antimicrobial activity analysis

The antibacterial activities of Au–Ag NPs, Au NPs, and bio-NPs against *E. coli*, *E. faecalis*, *P. aeruginosa*, *S. aureus*, and multi-culture strains were analyzed by MIC assay. No antibacterial effect was observed for Au NPs or bio-NPs at concentrations up to as high as 100 μM (data not shown). On the other hand, Au–Ag NPs showed considerable antibacterial activity at 30–50 μM concentrations for the used bacteria (refer to Table 1). It was found that as the concentration of Au–Ag NPs increased, the microbial growth was suppressed for all bacterial strains examined.

Table 1. ZI and MIC values of Au–Ag NPs against different pathogenic strains.

Bacterial strain	Au–Ag NPs (mm) 25 μM	Au–Ag NPs (mm) 50 μM	Streptomycin (mm) 50 μM	MIC (μM)
Gram-negative				
Escherichia coli	12	21	14	30
Pseudomonas aeruginosa	14	23	16	50
Gram-positive				
Enterococcus faecalis	13	20	NA	40
Staphylococcus aureus	*18*	*22*	NA	50
Multi-culture	19	23	11	40

Disk diffusion test results (Figure 6) were in good agreement with MIC test results. Au–Ag NPs produced a clear ZI that correlated with the antibiotic activity of streptomycin for Gram-negative, Gram-positive, and mixed bacteria. For LBA plates treated with *E. coli*, *E. faecalis*, *P. aeruginosa*, *S. aureus*, and multi-culture strains, clear ZIs were observed for Au–Ag NPs at concentrations of 20 and 50 μM (Figure 6 (a) to (e)). Furthermore, the diameter of ZIs (Table 1) of 50 μM Au–Ag NPs for all strains was >20 mm as compared with ZIs of ~14 mm for the streptomycin control. On the other hand, like untreated control, Au NPs and bio-NPs did not produce any considerable ZI at concentrations more than 50 μM (data not shown). Hence, it was noted that bacteria were less susceptible to Au NPs and bio-NPs than Au–Ag NPs.

Bioreduced NPs have found profuse utility in designing of novel therapeutic strategies against microbial infections. This study demonstrated that both

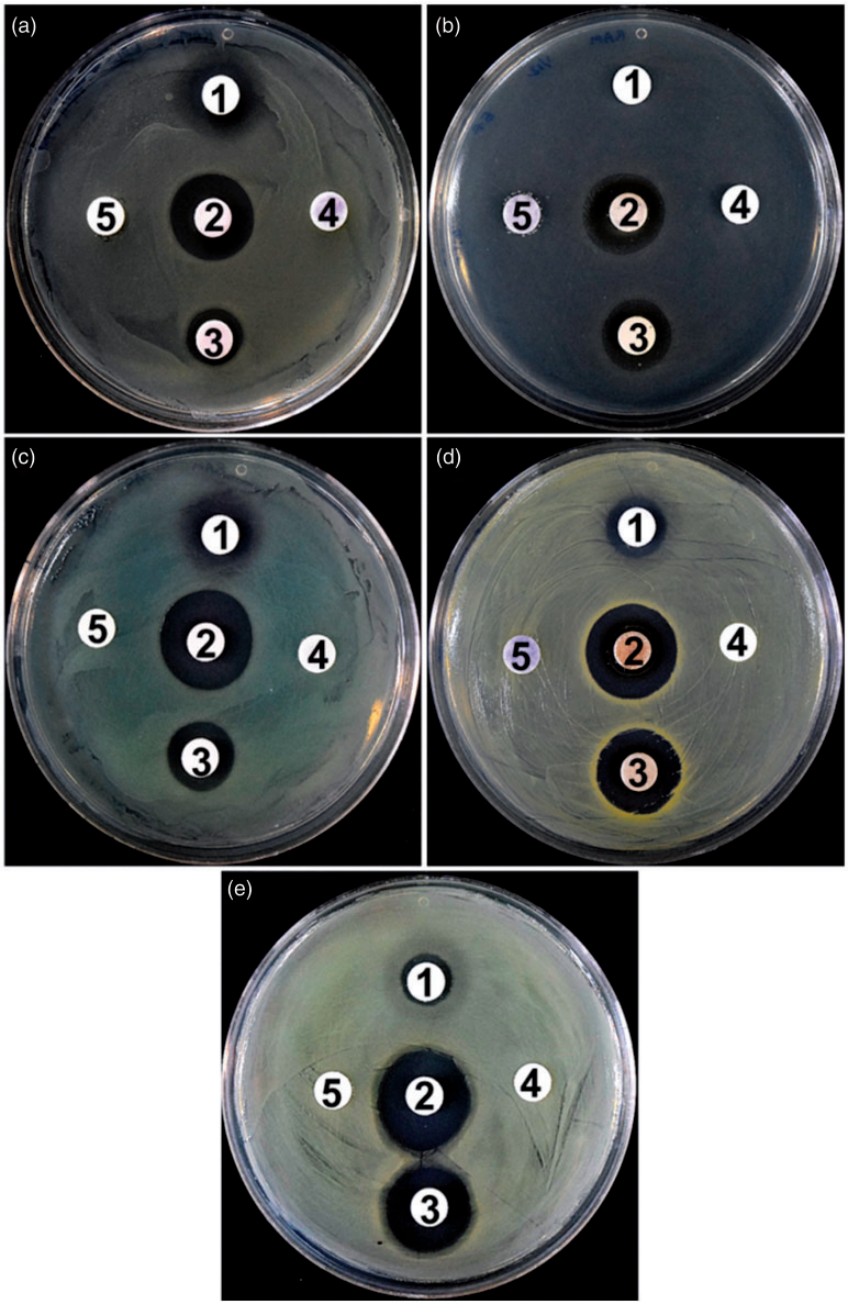

Figure 6. Disk diffusion assay results. Antibacterial activities of streptomycin (1), biofabricated Au–Ag NPs at 50 and 25 μM (2 and 3), Au NPs at 50 μM (4), and Bio-NPs at 50 μM (5) against *E. coli* (a), *E. faecalis* (b), *P. aeruginosa* (c), *S. aureus* (d) and multi-culture strains of all bacteria (e), are shown.

Gram-positive and Gram-negative microorganisms were susceptible to Au–Ag NPs, which might have been related to NP composition. Although Gram-negative bacteria have a lipopolysaccharide outer membrane which protects the bacteria from foreign substances like NPs, they are sensitive to the biocidal effects of Au–Ag NPs.[46] Based on MIC determinations it was concluded that Au–Ag NPs exhibited broad spectrum biocidal activity regardless of cell wall composition. Hence, there was no evidence of antibacterial activity for Au NPs, especially bio-NPs that are not composed of Ag in their particle structure. Furthermore, ZI is an indication of the biocidal potential of an agent, which suggests Au–Ag NPs released Ag (in an NP or metallic ion form) to cause a ZI. These results suggest Au–Ag NPs have promising broad spectrum antibacterial potential against pathogenic microorganisms than antibiotics.

Inhibition of biofilm formation by Au–Ag NPs

In the present study, we examined the effects of synthesized NPs on biofilm formation by *E. coli*, *E. faecalis*, *P. aeruginosa*, *S. aureus*, and multi-culture strains (Figure 7). Au–Ag NPs were seen to inhibit biofilm formation of all single strains and of multi-culture strains in a dose-dependent manner (Figure 7(a) to (e)). At concentrations of 10, 150, 100, 250, and 150 μM, Au–Ag NPs inhibited biofilm formation by *E. coli*, *E. faecalis*, *P. aeruginosa*, *S. aureus*, and multi-culture strains. Different patterns of biofilm formation activity were observed for Au NPs and bio-NPs where there has been no reduction in biofilm formation. In contrast, Au–Ag NPs showed remarkable biofilm disruption even at low concentrations (10 μM) for all the tested bacteria including mixed cultures. Mixed multi-culture biofilms were inhibited and disrupted by Au–Ag NPs to a greater extent than single bacterial biofilms, which might be due to the more penetration of NPs challenging their biofilm formation. The treated Au–Ag NPs could decrease the viable cell numbers that significantly arrested the synthesis of exopolysaccharides which is necessary for biofilm formation.[47,48] Also, different signaling mechanisms including quorum quenching could not rule out cell lysis process by Au–Ag NPs. This is the first report on biofilm inhibition activity of biofabricated Au–Ag NPs against *E. coli*, *E. faecalis*, *P. aeruginosa*, *S. aureus*, and multi-culture strains which was found to be superior activity as compared to Au NPs and bio-NPs.

Microscopic analysis of bactericidal effect

The possible mechanism of bacterial lysis by Au–Ag NPs was observed by FESEM and TEM. Fixed FESEM images of Au–Ag NP treated *E. coli*, *P. aeruginosa*, and *E. faecalis* are shown in Figure 8. In order to examine changes in morphology, two Gram-negative and one Gram-positive strains were selected. In comparison with control, Au NPs-treated bacteria showed different in contrast signals which explained the NPs attachment in the cells. Additionally, it can be clearly seen that the Au NPs significantly favored the formation of extra-cellular polymer matrix (EPS) than control. Further, magnified images of bacteria treated with Au NPs or control revealed regular, smooth surfaces without evidence of surface damage. In contrast, bacteria treated with Au–Ag NPs exhibited significant surface modifications. The low magnified images evidenced the severe cellular damage to the bacteria by depicting the irregular shape, discontinued population, and less EPS. Furthermore, high magnification exhibited the severity of cell damage, that is, loss of membrane integrity, wrinkling, rupture, and complete disintegration with loss of intracellular contents. After attachment, Au–Ag NPs could damage the cell membrane integrity by causing ''pits'' on the bacterial cell walls to enter inside the periplasm that initiated the cellular destruction. The high magnified images showed the presence of numerous ''pits'' on the bacteria surfaces made by the Au–Ag NPs which support the hypothesis. The penetrated Ag containing Au–Ag NPs could have caused further damage to the cell, possibly by interacting with sulfur- and phosphorous-containing cellular compounds such as DNA.[49] Hence, both, Gram-negative and Gram-positive strains, resulted in a complete surface disintegration against Au–Ag NPs regardless of its cellular composition.

To understand the interactions between *E. coli* and Au–Ag NPs, a cross-sectional TEM imaging experiment was performed (Figure 9). Au NP-treated bacteria (at 0.5 h) retained their cell structure, but Au–Ag NP-treated bacteria showed signs of cell damage initiation, such as intracellular voids and the disintegration of intracellular structures. The Figure 9 also shows that at 1 h, the internalizations of Au NPs and Au–Ag NPs had increased. Au NP-treated bacteria resembled untreated controls at all times, whereas Au–Ag NP-treated *E. coli* showed obvious morphological changes and appeared to undergo lysis with broken cell membranes and resulting loss of intracellular contents. The arrows in Figure 9 represent the degree of internalization of NPs with time and the severity of cellular damage. In particular, for Au–Ag NPs, NP uptake was low at 0.5 h and cell damage was slight, but further incubation of 1 and 1.5 h increased NP internalization and the severity of cell damage, and at 2 h cell *E. coli* disintegration was complete. The shape and size of the NPs are also responsible for antibacterial activity.[50] Since Au–Ag NPs were smaller, they provide more surface area that increased the possibility of NP-bacteria contact and hence caused potent bactericidal activity. The NPs internalization to the bacteria depends upon the nature of the bacterial cell wall and NPs. Here, less number of Au NPs or aggregates was attached in the bacteria at increasing time intervals as compared to Au–Ag NPs. The availability of bio-organic molecules around the Au–Ag NPs would be responsible for the attachment and internalization of NPs, even though the surface of the particles were negatively charged. The attached NPs could initially associate with lipopolysaccharides present in the lipid bilayers of bacterial cell membrane and thus cause NPs' penetration inside the cell. Further, high affinity of Ag (from Au–Ag NPs) with sulfur and phosphorus molecules inside the bacteria finally destroy the cell by inactivating the proteins and enzymes for ATP production which might be the key mechanism of Au–Ag NPs antibacterial property. The Au–Ag NPs penetrated bacteria, interact with DNA and regulating enzymes, impede electronic

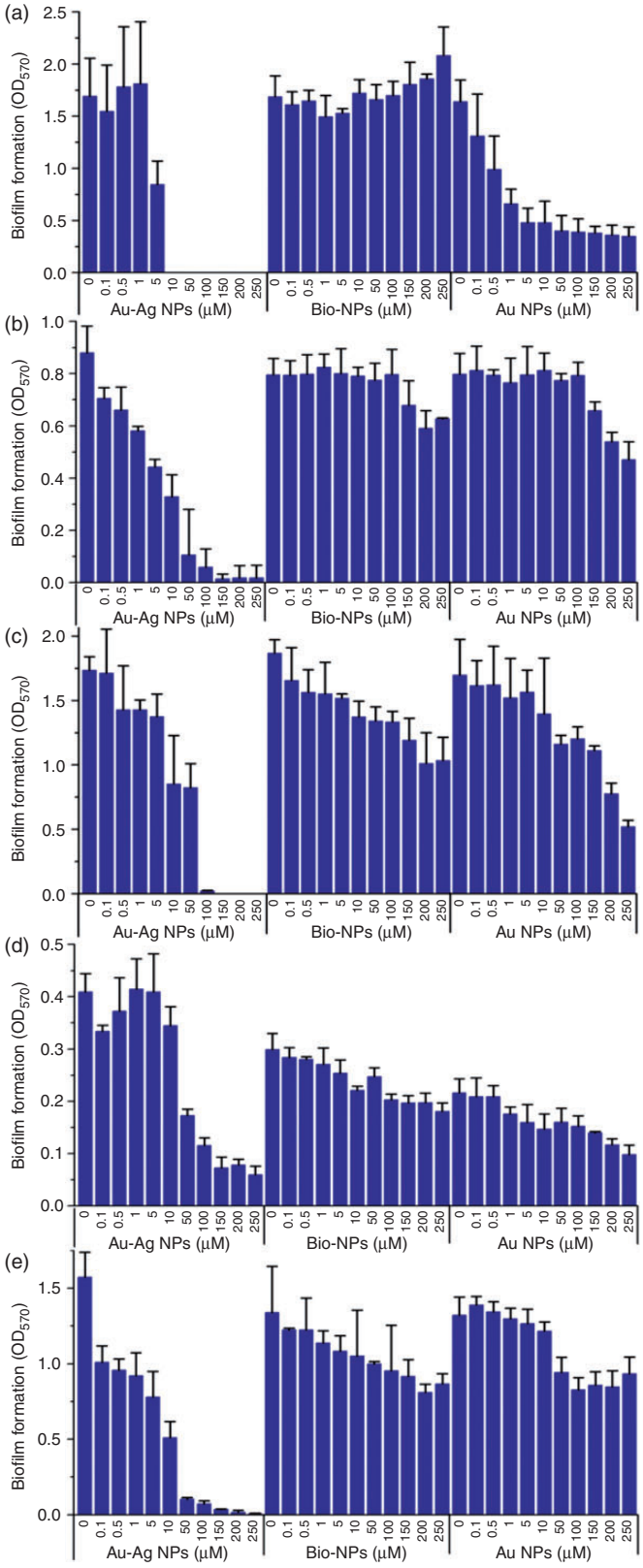

Figure 7. Effect of NPs on biofilm formation. The effects of different concentrations of Au–Ag NPs, Au NPs, and Bio-NPs on biofilm formation by *E. coli* (a), *E. faecalis* (b), *P. aeruginosa* (c), *S. aureus* (d), and multi-culture strains of all four bacteria (e) were examined after incubation in 96-well plates without shaking for 24 h. At least three independent experiments were conducted.

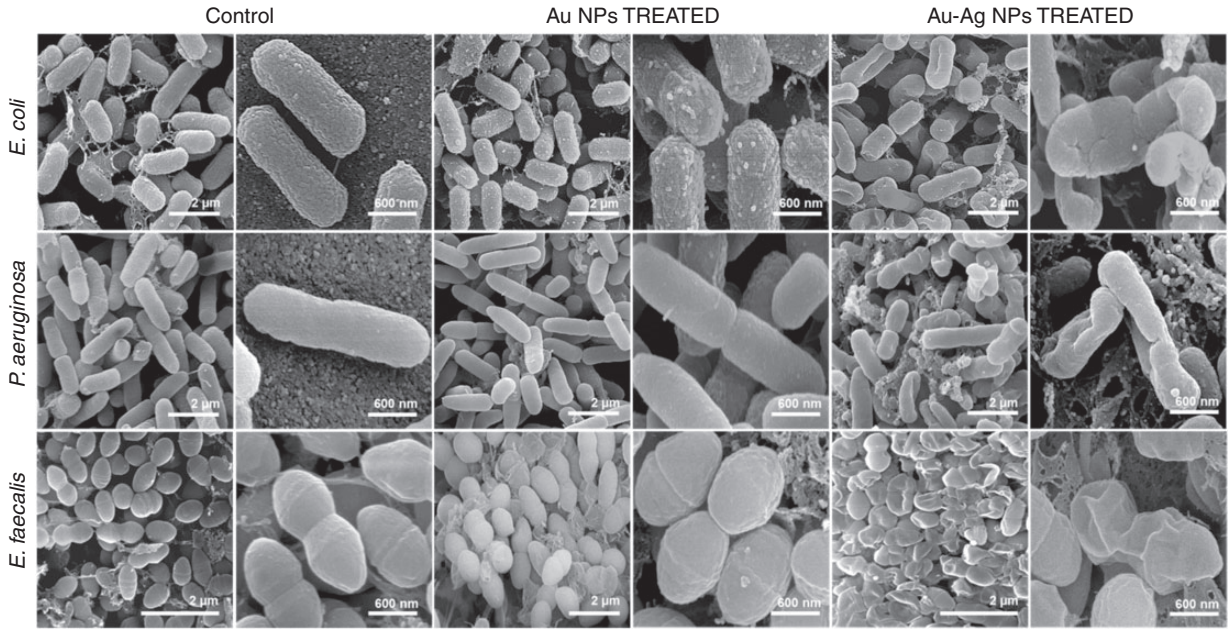

Figure 8. Morphologies of untreated and NP treated bacteria as determined by field emission scanning electron microscopy (FESEM). Low and high magnification images show the morphologic changes induced in *E. coli*, *E. faecalis*, and *P. aeruginosa* by Au NP and Au–Ag NPs-treated cells versus untreated controls.

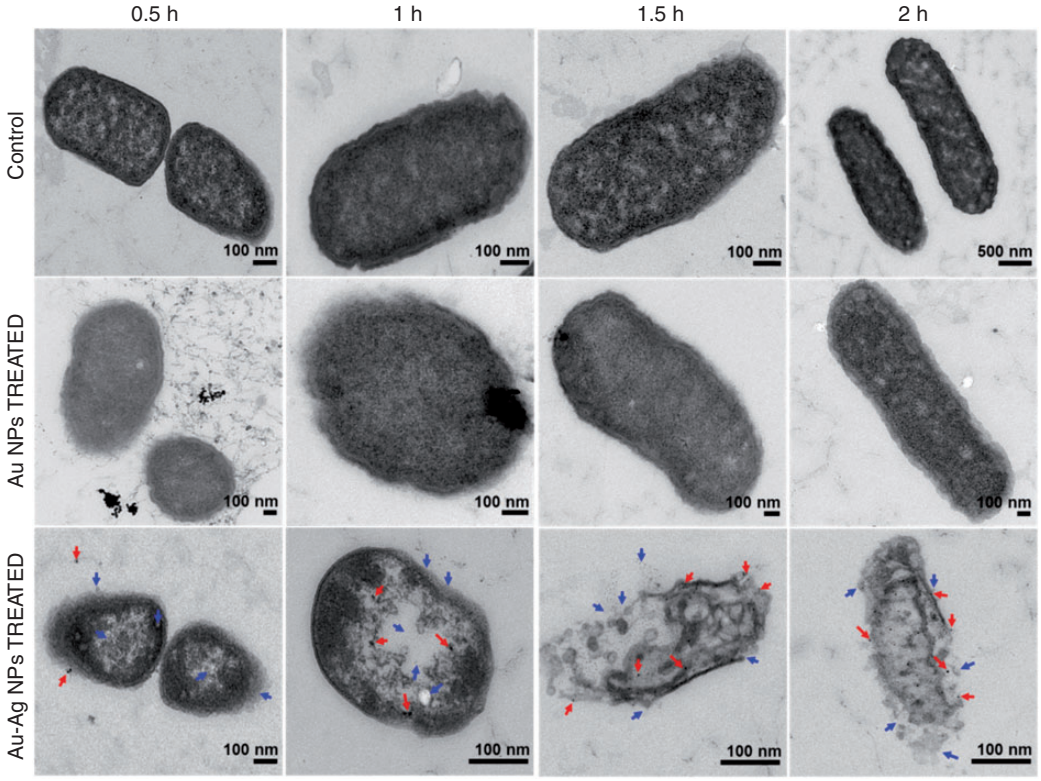

Figure 9. Transmission electron microscopy (TEM) findings of bacteria–NP interactions. Thin section of *E. coli* cells loaded with Au–Ag NPs, Au NPs, and non-treated NPs after 0.5 to 2 h of treatment. High magnification images showed the considerable time-dependent bactericidal effect of Au–Ag NPs. The red arrows show NPs in cells and the blue arrow indicates *E. coli* cells that have suffered irrecoverable damage.

transport, cause plasma membrane damage, and lead to cell lysis.[51,52]

The bacteriogenic synthesis approached here for Au–Ag NPs production is simple, cost effective, eco-friendly, and the formed NPs are highly stable. The Au–Ag NPs-cell surface interactions lead to more bacterial entrapment of NPs and the Ag present in the NPs might result in potent antimicrobial activity. The very smaller and spherical Au–Ag NPs penetrated through the biofilms and inhibited the entire bacteria populations even at low concentrations. The possible other antimicrobial mechanisms are further needed to be investigated.

Conclusions

In summary, this study described the antibacterial or antibiofilm activity of a biologically produced Au–Ag NPs using *S. oneidensis* MR-1 as bioreductant. Physical measurements suggested that the Au–Ag NPs formed were small in size (~20 nm), monodispersed, and highly stable in any solvents and that they were stabilized by a coating of microbial origin. Furthermore, Au–Ag NPs were found to have greater antimicrobial activity in a concentration-dependent manner. In addition, Au–Ag NPs were also found to be an effective biofilm inhibiting agent. Electron microscopy demonstrated the mechanism of Au–Ag NPs interaction with bacteria. We believe Au–Ag NPs offer a novel means of eradicating and biofilm formation by pathogenic bacteria and that these stable Au–Ag NPs might provide the basis for coating materials for surgical equipment's and wound dressing.

Declaration of Conflicting Interests

The author(s) declared no potential conflicts of interest with respect to the research, authorship, and/or publication of this article.

Funding

The author(s) disclosed receipt of the following financial support for the research, authorship, and/or publication of this article: This research was supported by a Yeungnam University research grant.

References

1. von Nussbaum F, Brands M, Hinzen B, et al. Antibacterial natural products in medicinal chemistry – exodus or revival? *Angew Chem Int Ed Engl* 2006; 45: 5072–5129.
2. Brady RA, Leid JG, Calhoun JH, et al. Osteomyelitis and the role of biofilms in chronic infection. *FEMS Immunol Med Microbiol* 2008; 52: 13–22.
3. Costerton JW, Stewart PS and Greenberg EP. Bacterial biofilms: a common cause of persistent infections. *Science* 1999; 284: 1318–1322.
4. Richards JJ and Melander C. Controlling bacterial biofilms. *Chem Bio Chem* 2009; 10: 2287–2294.
5. Simões M, Simões LC and Vieira MJ. A review of current and emergent biofilm control strategies. *LWT – Food Sci Technol* 2010; 43: 573–583.
6. Hajipour MJ, Fromm KM, Ashkarran AA, et al. Antibacterial properties of nanoparticles. *Trends Biotechnol* 2012; 30: 499–511.
7. Azam A, Ahmed AS, Oves M, et al. Antimicrobial activity of metal oxide nanoparticles against Gram-positive and Gram-negative bacteria: a comparative study. *Int J Nanomed* 2012; 7: 6003–6009.
8. Ramasamy M, Lee SS, Yi DK, et al. Magnetic, optical gold nanorods for recyclable photothermal ablation of bacteria. *J Mater Chem B Mater Biol Med* 2014; 2: 981–988.
9. Thiel J, Pakstis L, Buzby S, et al. Antibacterial properties of silver-doped titania. *Small* 2007; 3: 799–803.
10. Gunawan P, Guan C, Song X, et al. Hollow fiber membrane decorated with Ag/MWNTs: toward effective water disinfection and biofouling control. *ACS Nano* 2011; 5: 10033–10040.
11. Agnihotri S, Mukherji S and Mukherji S. Immobilized silver nanoparticles enhance contact killing and show highest efficacy: elucidation of the mechanism of bactericidal action of silver. *Nanoscale* 2013; 5: 7328–7340.
12. Hu C, Liu S, Li B, et al. Micro-/nanometer rough structure of a superhydrophobic biodegradable coating by electrospraying for initial anti-bioadhesion. *Adv Healthc Mater* 2013; 2: 1314–1321.
13. Wang G-H, Hilgert J, Richter FH, Wang F, et al. Platinum–cobalt bimetallic nanoparticles in hollow carbon nanospheres for hydrogenolysis of 5-hydroxymethylfurfural. *Nat Mater* 2014; 13: 293–300.
14. Moghimi N, Mohapatra M and Leung KT. Bimetallic nanoparticles for arsenic detection. *Anal Chem* 2015; 87: 5546–5552.
15. Shi Y, Lin M, Jiang X, et al. Recent advances in FePt nanoparticles for biomedicine. *Biomedicine* 2015; 21: 22.
16. Kumar R, Gokulakrishnan N, Kumar R, et al. Can be a bimetal Oxide ZnO–MgO nanoparticles anticancer drug carrier and deliver? Doxorubicin adsorption/release study. *J Nanosci Nanotechnol* 2015; 15: 1543–1553.
17. Banerjee M, Sharma S, Chattopadhyay A, et al. Enhanced antibacterial activity of bimetallic gold-silver core–shell nanoparticles at low silver concentration. *Nanoscale* 2011; 3: 5120–5125.
18. Mallin MP and Murphy CJ. Solution-phase synthesis of sub-10 nm Au-Ag alloy nanoparticles. *Nano Lett* 2002; 2: 1235–1237.
19. Sanchez-Ramirez J, Pal U, Nolasco-Hernandez L, et al. Synthesis and optical properties of Au-Ag alloy nanoclusters with controlled composition. *J Nanomat* 2008; 2008: 9.
20. Chen Y-H and Yeh C-S. A new approach for the formation of alloy nanoparticles: laser synthesis of gold–silver alloy from gold–silver colloidal mixtures. *Chem Commun (Camb)* 2001; 4: 371–372.
21. Treguer M, de Cointet C, Remita H, et al. Dose rate effects on radiolytic synthesis of gold-silver bimetallic clusters in solution. *J Phys Chem B* 1998; 102: 4310–4321.
22. Tsai T-H, Thiagarajan S and Chen S-M. Ionic liquid assisted one step green synthesis of Au–Ag bimetallic nanoparticles. *J Appl Electrochem* 2010; 40: 493–497.

23. Mizukoshi Y, Fujimoto T, Nagata Y, et al. Characterization and catalytic activity of core-shell structured gold/palladium bimetallic nanoparticles synthesized by the sonochemical method. *J Phys Chem B* 2000; 104: 6028–6032.
24. Sheny D, Mathew J and Philip D. Phytosynthesis of Au, Ag and Au–Ag bimetallic nanoparticles using aqueous extract and dried leaf of *Anacardium occidentale*. *Spectrochim Acta A Mol Biomol Spectrosc* 2011; 79: 254–262.
25. Singh S, Vidyarthi AS and Dev A. Microbial Synthesis of Nanoparticles. In: Singh OV (eds) *Bio-Nanoparticles: Biosynthesis and Sustainable Biotechnological Implications*. Hoboken, NJ: John Wiley & Sons, Inc, 2015, pp. 155–179.
26. Thakkar KN, Mhatre SS and Parikh RY. Biological synthesis of metallic nanoparticles. *Nanomed Nanotechnol Biol Med* 2010; 6: 257–262.
27. Suresh AK, Pelletier DA, Wang W, et al. Biofabrication of discrete spherical gold nanoparticles using the metal-reducing bacterium *Shewanella oneidensis*. *Acta Biomater* 2011; 7: 2148–2152.
28. De Corte S, Hennebel T, Fitts JP, et al. Biosupported bimetallic Pd–Au nanocatalysts for dechlorination of environmental contaminants. *Environ Sci Technol* 2011; 45: 8506–8513.
29. Senapati S, Ahmad A, Khan MI, et al. Extracellular biosynthesis of bimetallic Au–Ag alloy nanoparticles. *Small* 2005; 1: 517–520.
30. Zheng D, Hu C, Gan T, et al. Preparation and application of a novel vanillin sensor based on biosynthesis of Au–Ag alloy nanoparticles. *Sensors Actuators B Chem* 2010; 148: 247–252.
31. Narayanan KB and Sakthivel N. Biological synthesis of metal nanoparticles by microbes. *Adv Colloid Interface Sci* 2010; 156: 1–13.
32. Singh P, Kim Y-J, Zhang D, et al. Biological synthesis of nanoparticles from plants and microorganisms. *Trends Biotechnol*. Epub ahead of print 2 May 2016. DOI: 10.1016/j.tibtech.2016.02.006.
33. Kalathil S, Lee J and Cho MH. Electrochemically active biofilm-mediated synthesis of silver nanoparticles in water. *Green Chem* 2011; 13: 1482–1485.
34. Frens G. Controlled nucleation for the regulation of the particle size in monodisperse gold suspensions. *Nature* 1973; 241: 20–22.
35. Kim Y-G, Lee J-H, Cho MH, et al. Indole and 3-indolylacetonitrile inhibit spore maturation in *Paenibacillus alvei*. *BMC Microbiol* 2011; 11: 119.
36. Ji Y, Yang S, Guo S, et al. Bimetallic Ag/Au nanoparticles: a low temperature ripening strategy in aqueous solution. *Colloids Surf A Physicochem Eng Asp* 2010; 372: 204–209.
37. Qian L and Yang X. Preparation and characterization of Ag (Au) bimetallic core–shell nanoparticles with new seed growth method. *Colloids Surf Physicochem Eng Aspects* 2005; 260: 79–85.
38. Shannahan JH, Lai X, Ke PC, et al. Silver nanoparticle protein corona composition in cell culture media. *PLoS One* 2013; 8: e74001.
39. Fredrickson JK, Romine MF, Beliaev AS, et al. Towards environmental systems biology of *Shewanella*. *Nat Rev Microbiol* 2008; 6: 592–603.
40. Kumar SA, Abyaneh MK, Gosavi SW, et al. Sulfite reductase-mediated synthesis of gold nanoparticles capped with phytochelatin. *Biotechnol Appl Biochem* 2007; 47: 191–195.
41. Marsili E, Baron DB, Shikhare ID, et al. *Shewanella* secretes flavins that mediate extracellular electron transfer. *Proc Natl Acad Sci* 2008; 105: 3968–3973.
42. Ghosh S, Jagtap S, More P, et al. *Dioscorea bulbifera* mediated synthesis of novel Au core Ag shell nanoparticles with potent antibiofilm and antileishmanial activity. *J Nanomater* 2015; 10: 7477–7490.
43. Kumari MM, Jacob J and Philip D. Green synthesis and applications of Au–Ag bimetallic nanoparticles. *Spectrochim Acta A Mol Biomol Spectrosc* 2015; 137: 185–192.
44. Shin Y, Bae I-T, Arey BW, et al. Facile stabilization of gold-silver alloy nanoparticles on cellulose nanocrystal. *J Phys Chem C* 2008; 112: 4844–4848.
45. Philip D. Biosynthesis of Au, Ag and Au–Ag nanoparticles using edible mushroom extract. *Spectrochim Acta A Mol Biomol Spectrosc* 2009; 73: 374–381.
46. Amro NA, Kotra LP, Wadu-Mesthrige K, et al. High-resolution atomic force microscopy studies of the *Escherichia coli* outer membrane: structural basis for permeability. *Langmuir* 2000; 16: 2789–2796.
47. Ansari MA, Maayah ZH, Bakheet SA, et al. The role of aryl hydrocarbon receptor signaling pathway in cardiotoxicity of acute lead intoxication in vivo and in vitro rat model. *Toxicology* 2013; 306: 40–49.
48. Machul A, Mikołajczyk D, Regiel-Futyra A, et al. Study on inhibitory activity of chitosan-based materials against biofilm producing *Pseudomonas aeruginosa* strains. *J Biomater Appl* 2015; 30: 269–278.
49. Gibbins B and Warner L. The role of antimicrobial silver nanotechnology. *Med Device Diagnostic Indust Mag* 2005; 1: 1–2.
50. Baker C, Pradhan A, Pakstis L, et al. Synthesis and antibacterial properties of silver nanoparticles. *J Nanosci Nanotechnol* 2005; 5: 244–249.
51. Su H-L, Chou C-C, Hung D-J, et al. The disruption of bacterial membrane integrity through ROS generation induced by nanohybrids of silver and clay. *Biomaterials* 2009; 30: 5979–5987.
52. Das B, Dash SK, Mandal D, et al. Green synthesized silver nanoparticles destroy multidrug resistant bacteria via reactive oxygen species mediated membrane damage. *Arabian J Chem*. Epub ahead of print 21 August 2015. DOI: 10.1016/j.arabjc.2015.08.008.